CHINA FOUNDRY Research & Development
Vol. 23 No. 3 May 2026
www.springer.com/41230
https://doi.org/10.1007/s41230-026-5156-8

Effect of eutectic content on microstructure and mechanical properties of Al-Zn-Mg-Cu alloys

Peng-fei Li[1,2], *Yu-dong Sui[1,2], Hai-ni Jin[1,2], An-kang Xiong[1,2], Wan-zeng Li[1,2], Hao Zhou[3], and **Ye-hua Jiang[1,2]

1. Faculty of Materials Science and Engineering, Kunming University of Science and Technology, Kunming 650093, China

2. National-Local Joint Engineering Laboratory for Technology of Advanced Metallic Solidification Forming and Equipment, Kunming University of Science and Technology, Kunming 650093, China

3. Liaoning Academy of Materials, Shenyang 110167, China

Copyright © 2026 Foundry Journal Agency

Abstract: The 7xxx series aluminum alloys have emerged as a particularly promising class of lightweight structural materials. However, the inherent strength of these materials is primarily influenced by the content and type of alloying elements added during the manufacturing process, as well as casting defects. The present study investigated the effects of eutectics formed by solute atoms (Zn, Mg, and Cu), with equal mass ratios (Zn/Mg=2, Mg/Cu=3) but varying overall contents, on the liquid film thickness, crack propagation depth, and the mechanical properties of the Al-Zn-Mg-Cu alloy after heat treatment. The results from gravity casting indicate that the intergranular liquid film thickness increases with the increase of eutectic content. A thick intergranular liquid film in the casting can accommodate greater strain during grain contraction, thereby preventing liquid film rupture and subsequent hot tearing. Concurrently, during the solution treatment at 475 °C, the residual eutectic fraction in the Al-7Zn-3.5Mg-1.18Cu alloy diminishes from 9.1% at 10 h to 0.35% at 40 h. At 165 °C, the Al-6Zn-3.0Mg-1.0Cu alloy exhibits the optimal mechanical properties, with a peak aging tensile strength of 510 MPa and an elongation of 6.4%. The incorporation of lower concentrations of solute atoms (Zn, Mg, and Cu) serves to reduce the barrier to dislocation precipitation, thereby enhancing alloy plasticity. However, when the proportion of alloying elements exceeds the solubility limit of the α-Al matrix at specific heat treatment temperatures, coarse residual phases remain intergranular, thereby significantly impairing the mechanical properties of the alloy. This study provides a reference for the optimal addition level of the main strengthening elements in Al-Zn-Mg-Cu alloys.

Keywords: Al-Zn-Mg-Cu alloy; eutectic content; tensile strength; thickness of liquid film; hot tearing susceptibility

CLC numbers: TG146.21 **Document code:** A **Article ID:** 1672-6421(2026)03-462-13

1 Introduction

Aluminum alloys are of particular interest due to their low density, high specific strength, and excellent corrosion resistance, which make them highly promising lightweight structural materials in aerospace, rail transportation, and automotive lightweighting applications[1-4]. Nevertheless, this series of alloys generally exhibits poor castability, and their mechanical properties mainly rely on the synergistic strengthening effect of major alloying elements such as Zn, Mg, and Cu. Nano-sized second phases can be precipitated from Zn and Mg after solution treatment and aging, thereby achieving a remarkable age-hardening effect[5-7]. Therefore, balancing the relationship between castability and mechanical properties has become a research hotspot in this field.

The ratio of primary alloying elements, such as Zn, Mg, and Cu, along with their solid solution behavior in the aluminum matrix, is a key factor determining the type, size, volume fraction, and spatial distribution of precipitation phases. These factors directly influence the overall properties

***Yu-dong Sui**

Male, born in 1986, Ph. D., Professor. Research interests: Aluminum, magnesium, and other light alloy materials and their forming technologies. His academic research has led to the publication of more than 50 technical papers.

E-mail: suiyudong@126.com

****Ye-hua Jiang**

Male, born in 1968, Ph. D., Professor. His research interests include casting technology, additive manufacturing, and development of wear-resistant materials, and composites.

E-mail: jiangyehua@kmust.edu.cn

Received: 2025-07-09; Revised: 2025-10-16; Accepted: 2026-05-13

of alloys[8-10]. Of particular significance is the equilibrium solubility limits of these elements in the Al matrix, which are pivotal to achieving effective solid solution strengthening. However, during the process of solidification, the presence of non-equilibrium solidification leads to the accumulation of solute atoms (e.g., Zn, Mg, Cu) at the solid-liquid interface. This results in the formation of a eutectic microstructure at the end of the solidification process. Consequently, these solute atoms are unable to achieve maximum solubility in the Al matrix. Therefore, a subsequent solution treatment is generally required to maximize the solubility of solute atoms (Zn, Mg, Cu) in the Al matrix and enhance the strength of alloys[11]. However, when elemental content exceeds this limit, excess elements tend to form coarse, insoluble secondary phases, leading to a sharp deterioration in mechanical properties. In the case of 7xxx alloys, the incorporation of alloying elements (e.g., Zr, Ti, Ce) and nanoparticles has been demonstrated to enhance mechanical properties by refining grain size and forming secondary phases[12-14]. As reported by Akuata et al.[15], the addition of Ag resulted in the formation of Ag-rich AlAgZnMgCu phases; however, it did not enhance the properties of the 7xxx alloys with a Zn/Mg ratio of 4. Nevertheless, given the strengthening effect and cost advantages, it is imperative to optimize the influence of primary alloying elements.

The solution behavior of secondary phases in as-cast microstructures is closely related to the solution temperature and time. Solution temperature determines the maximum solid solubility and accommodating capacity of the aluminum matrix for solute atoms, whereas solution time governs the kinetic process of solute diffusion and dictates the dissolution extent of residual second phases as well as the homogenization effect. These two factors jointly influence the solid solution degree of solute atoms and the subsequent age-precipitation behavior of the alloy[16, 17]. Nevertheless, in Al-Zn-Mg-Cu alloys, the selection of solution treatment temperature is mainly determined by the melting temperature of the low melting eutectic phase. To achieve sufficient dissolution of solute atoms into the matrix via solid state diffusion while avoiding incipient melting, solution time, serves as a crucial parameter in heat treatment processing, must be carefully controlled. The dissolution of poorly soluble coarse phases is facilitated by extending the solution treatment time, thereby increasing the actual solubility of the matrix[18, 19]. The solid solution process of Zn, Mg, and Cu in aluminum matrices is primarily governed by the diffusion kinetics of each element and the dissolution rate of the second phase[20]. Among these elements, Cu atoms typically govern the solid solution time due to their high diffusion activation energy and low diffusion coefficient. The dissolution time of coarse Al_2CuMg (S phase) is shown to be considerably prolonged under certain conditions[21, 22].

In recent years, optimization research on cast Al-Zn-Mg-Cu alloys has been focused on regulating the Zn/Mg/Cu element ratios to synergistically optimize microstructures through solution treatment and aging processes. This approach has been shown to balance strength, ductility, and corrosion resistance[21-23]. Nevertheless, critical scientific issues persist regarding as-cast 7xxx series aluminum alloys: Firstly, there is a paucity of systematic research on the quantitative relationship between maximum equilibrium solid solubility of alloying elements and solid solution time in multi-component systems. In particular, the mechanism underlying the influence of multi-element interactions on the solid solubility limit remains unclear. Secondly, as materials sensitive to solidification defects, hot tearing susceptibility (HTS) remains a core constraint for their large-scale casting applications[24, 25]. As demonstrated in previous studies[26], the eutectic phase content exerts a substantial influence on the susceptibility of alloys to hot tearing. However, critical hot tearing characteristics, including liquid film thickness, remain a subject of limited exploration. Additionally, it is crucial to acknowledge that, given the primary function of Al-Zn-Mg-Cu alloys as load-bearing components, their overall properties are more influenced by the mechanical response following solution treatment and aging.

Consequently, this study proposed a dual-action mechanism for the eutectic phase, which involves the regulation of hot tearing susceptibility during the casting stage and the influence of the morphology and distribution of the unsolved phase during the solution treatment and aging stage on strengthening effects. A series of casting alloys with varying eutectic contents were designed. A comprehensive investigation was conducted, integrating solution treatment-aging processes with microstructural characterization to explore the impact of eutectic content on liquid film thickness and crack propagation depth. It examined the mechanism underlying the effects of heat treatment on strength and toughness, as well as synergistic control strategies for hot tearing susceptibility and mechanical properties. By elucidating the intrinsic influence of eutectic content on alloy properties through the solution-aging pathway, this work provides theoretical and process design foundations for developing novel cast aluminum alloys featuring low hot tearing susceptibility, high strength and toughness, and a broad process window.

2 Materials and experimental procedure

To maintain the type of second phases unchanged, the alloys were designed with a Zn/Mg mass ratio of 2 and a Mg/Cu mass ratio of 3. After weighing the raw materials according to the designed alloy composition, the alloy was melted in a medium-frequency electromagnetic induction furnace. Initially, pure Al and the Al-50Cu intermediate alloy were introduced to a graphite clay crucible. Following a thorough melting process, the temperature was decreased to 690 °C prior to the introduction of pure Zn and pure Mg. Subsequently, pure Zn and pure Mg were subjected to a process of full melting, followed by an elevation in temperature to 730 °C, and held for 30 min. Subsequently, the slag was removed, and the molten metal was poured into separate metal molds. The

gravity casting experiments utilized metal molds fabricated from 45 steel, with the shapes and dimensions depicted in Fig. 1(a). The bottom-pouring method was employed in the casting process, and the molds were to be preheated to 150 °C prior to casting. To compensate for element loss during melting, pure Mg (15wt.% excess) and pure Zn (3wt.% excess) were added on the basis of the nominal Mg and Zn contents. The chemical composition of the alloys was determined using an inductively coupled plasma optical emission spectrometer (ICP-OES: 5800, Agilent), and delineated in Table 1. All samples were solution treated at 475 °C for 30 h. The age-hardening curves at 165 °C during artificial aging were then measured using a Vickers hardness tester (HVS-1000AT). Subsequently, the peak-aged tensile strength was achieved.

Microstructural characterization of the samples was performed using a Zeiss EVO 180 scanning electron microscope (SEM). The area fraction of eutectic regions [Position 2 in Fig. 1(b)] and the liquid film thickness on hot tearing fracture surfaces were statistically analyzed using Image-Pro Plus software. Phase identification was carried out by Rigaku Mini Flex 600 X-ray diffractometer (XRD) at 20°–80° with a scanning rate of 5°·min^{-1}. Same position of each sample [(Position 1 in Fig. 1(b)] was cut via wire electrical discharge machining (wire-EDM). The geometry and dimensions of the tensile specimens are illustrated in Fig. 1(d). Prior to testing, the tensile specimens were ground and polished to achieve a smooth and flat surface. Tensile tests were conducted on the MTS-E45.305 universal testing machine according to the national standard for tensile testing of metallic materials (GB/T 228.1-2010), at a tensile rate of 1 mm·min^{-1}. Three specimens were selected for each test group, with results averaged. Hot tearing fracture morphology was obtained using a constraint

Table 1: Chemical compositions of experimental alloys (wt.%)

Designation	Alloy	Al	Zn	Mg	Cu	Zr	Sc	Mg/Cu ratio
Zn12	Al-12Zn-6.0Mg-2.0Cu	Bal.	11.8±0.2	6.0±0.2	1.9±0.08	0.10	0.10	3
Zn10	Al-10Zn-5.0Mg-1.67Cu	Bal.	10.2±0.1	5.0±0.1	1.7±0.07	0.10	0.10	3
Zn8	Al-8Zn-4.0Mg-1.33Cu	Bal.	8.0±0.1	4.2±0.1	1.3±0.05	0.09	0.09	3
Zn7	Al-7Zn-3.5Mg-1.18Cu	Bal.	7.2±0.1	3.6±0.1	1.1±0.04	0.10	0.10	3
Zn6	Al-6Zn-3.0Mg-1.0Cu	Bal.	6.0±0.1	3.1±0.1	1.0±0.05	0.09	0.09	3
Zn4	Al-4Zn-2.0Mg-0.67Cu	Bal.	4.0±0.2	2.0±0.1	0.65±0.10	0.09	0.10	3

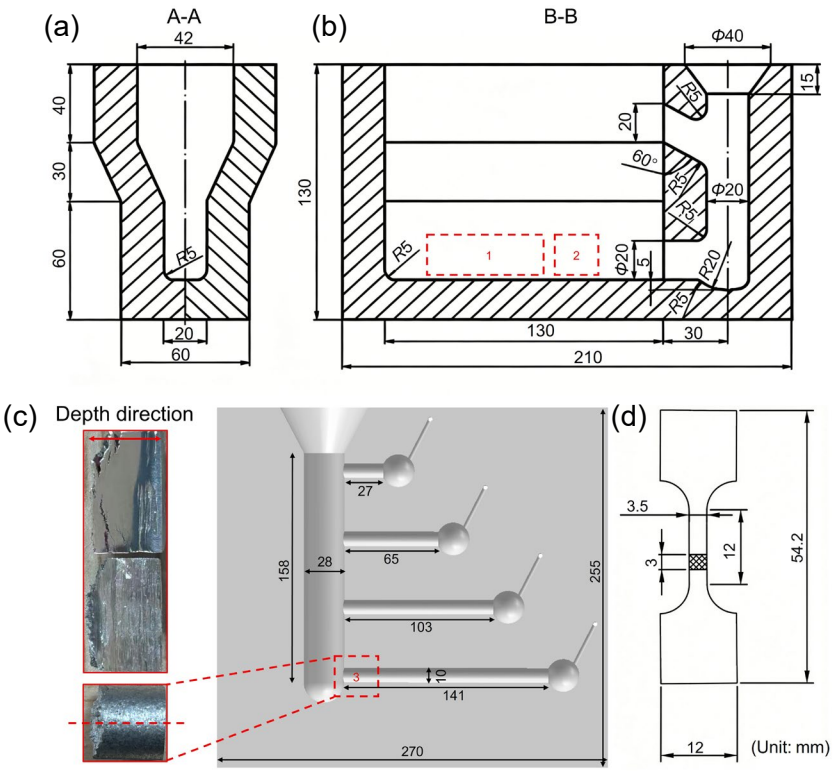

Fig. 1: Shape and size of metal mold (a–b), hot tearing test mold and sampling location diagram (c), and shape and size of tensile specimen (d)

rod test mold, with sampling at Position 3 marked in Fig. 1(c). The solidification path of the alloy under equilibrium conditions was calculated using Thermo-Calc software. The average thermal expansion coefficient and surface tension of the alloy were calculated using JMatPro software. The DSC curve of the Zn7 alloy was measured by differential scanning calorimetry using a simultaneous thermal analyzer (TGA/DSC1/1600).

3 Results and discussion

3.1 Microstructure of alloy analysis

Figure 2 shows equilibrium phase fraction diagrams of alloys with different eutectic contents plotted using Thermo Calc software. As the temperature decreases, the Al_3Zr and Al_3Sc phases with higher melting points first form from the liquid. Subsequently, the volume fraction of α-Al gradually increases as the temperature decreases. During the solid-state diffusion process, the volume fraction of α-Al gradually decreases. Figure 2(a) depicts the solidification process of Zn12 alloy, the maximum volume fraction of α-Al that forms during solidification is 0.9. The remaining melt transforms directly into a eutectic phase during the final stage of solidification. Since solute diffusion coefficients are smaller in the solid phase, the temperature drops significantly before solute diffusion can occur. This causes the solid-liquid interface to advance substantially, allowing new solid phases to crystallize. Ultimately, solute atoms (Zn, Mg, and Cu) become enriched at the interface.

As the incorporation of alloying elements (Zn, Mg, and Cu) is reduced, the volume fraction of α-Al approaches 0.98 at Zn8 alloy. At this stage, the remaining melt directly transforms into a eutectic microstructure during the final stage of solidification. In the Zn7, Zn6, and Zn4 alloys, all solute atoms are completely dissolved into the matrix during solidification, forming a supersaturated α-Al solid solution. Consequently, no eutectic phases form at the solid-liquid interface, resulting in an α-Al fully phase. However, the solubility of alloying elements (Zn, Mg, and Cu) in the α-Al matrix decreases with decreasing temperature. As a result, these solute elements precipitate from the α-Al matrix, forming eutectic structures dominated by solid-state diffusion. In addition, theoretical calculations reveal that the liquidus of the alloy decreases with increasing additions of Zn, Mg, and Cu. This phenomenon can be attributed to the fact that higher solute contents shift the actual composition at the solid-liquid interface closer to that of the solid phase, thereby lowering the liquidus.

Figure 3 shows the XRD patterns of the alloys with different additions of solute elements (Zn, Mg, and Cu). The main diffraction peaks correspond to the (111), (200), (220), and (311) crystal planes of the Al matrix. The predominant Al matrix peak, accompanied by variable secondary diffraction peaks, unmistakably signifies the impact of the aggregate solute element (Zn, Mg, and Cu) content on the development of secondary phases within the microstructure of the as-cast Al alloy. The fundamental mechanism is rooted in disparities in solute partitioning and phase transformation kinetics during the solidification process. In instances of elevated solute element additions (for instance, Zn12 alloy), under conditions of non-equilibrium solidification, solute elements (particularly

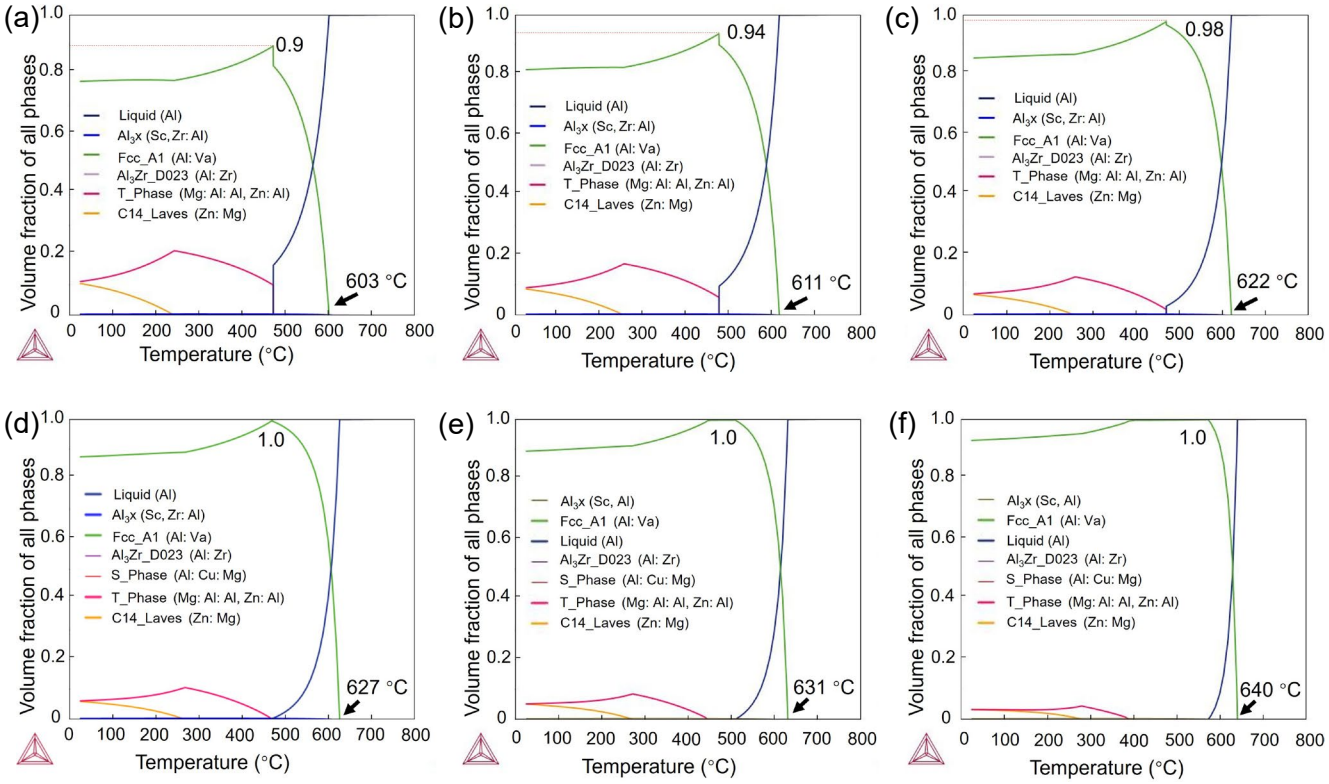

Fig. 2: Equilibrium phase fraction diagrams for alloys with different eutectic contents: (a) Zn12; (b) Zn10; (c) Zn8; (d) Zn7; (e) Zn6; (f) Zn4

Zn, Mg, and Cu with partition coefficients $k<1$) undergo substantial retention and enrichment in the liquid phase at the solid-liquid interface front. As the solidification process continues, the solute concentration in the residual liquid phase between dendrites continuously increases, eventually reaching the composition of the non-equilibrium eutectic point for that alloy system (e.g., the eutectic composition of the Al+T phase in the Al-Zn-Mg system). This prompts a non-equilibrium eutectic reaction, which in turn generates a substantial quantity of intermetallic compound secondary phases (e.g., the observed $Mg_{32}Zn_{31.9}Al_{17.1}$, the T phase). Conversely, when the total solute element addition is low, solute enrichment at the solid-liquid interface front during solidification is insufficient to reach the critical concentration required to trigger non-equilibrium eutectic reactions. The process of solidification primarily results in the formation of a single-phase α-Al supersaturated solid solution.

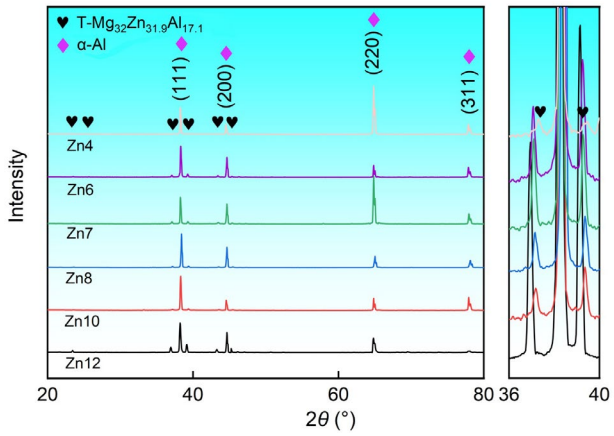

Fig. 3: XRD results of as-cast alloys containing different eutectic contents

During subsequent cooling, the supersaturated solid solutions form equilibrium second phases through solid-state precipitation. However, the small thermodynamic driving force (degree of supersaturation), and the low diffusion coefficients of elements such as Zn, Mg, and Cu in α-Al collectively result in an extremely low nucleation rate and an exceptionally slow growth rate for the precipitation process. Therefore, under conventional as-cast cooling conditions, it is difficult to form sufficient quantities of equilibrium secondary phases that can be clearly detected by XRD. Only extremely fine and dispersed early-stage precipitates (such as η, S, T phases, and GP regions) are likely to form[17].

Figures 4(a–f) show SEM images of the alloys. Black α-Al grains and white eutectic microstructure are clearly visible, with the eutectic microstructure growing along the α-Al grain boundaries. The area fraction of the eutectic microstructure within the Al matrix was quantified. As the mass fraction of the added solutes (Zn, Mg, and Cu) decreases, the area of the white eutectic microstructure gradually diminishes. The area fraction of eutectic T phases in the Zn12 alloy reaches 21.4%, whereas that in the Zn4 alloy is merely 1.8%. The area proportion of T phases is closely correlated with the addition level of solute atoms (Zn, Mg, and Cu). The higher solute content results in more extensive eutectic microstructures. At a constant cooling rate, the limited solid solubility of α-Al leads to an increased solute concentration ahead of the solid-liquid interface during solidification with the rising solute content, thereby forming a mushy zone. The subsequent solidification of the mushy zone eventually results in the formation of eutectic microstructures. Meanwhile, the solute atoms rejected from the solid phase accumulate at the interface, increasing the resistance to grain growth. A higher solute content thus further refines the grain size of the alloy.

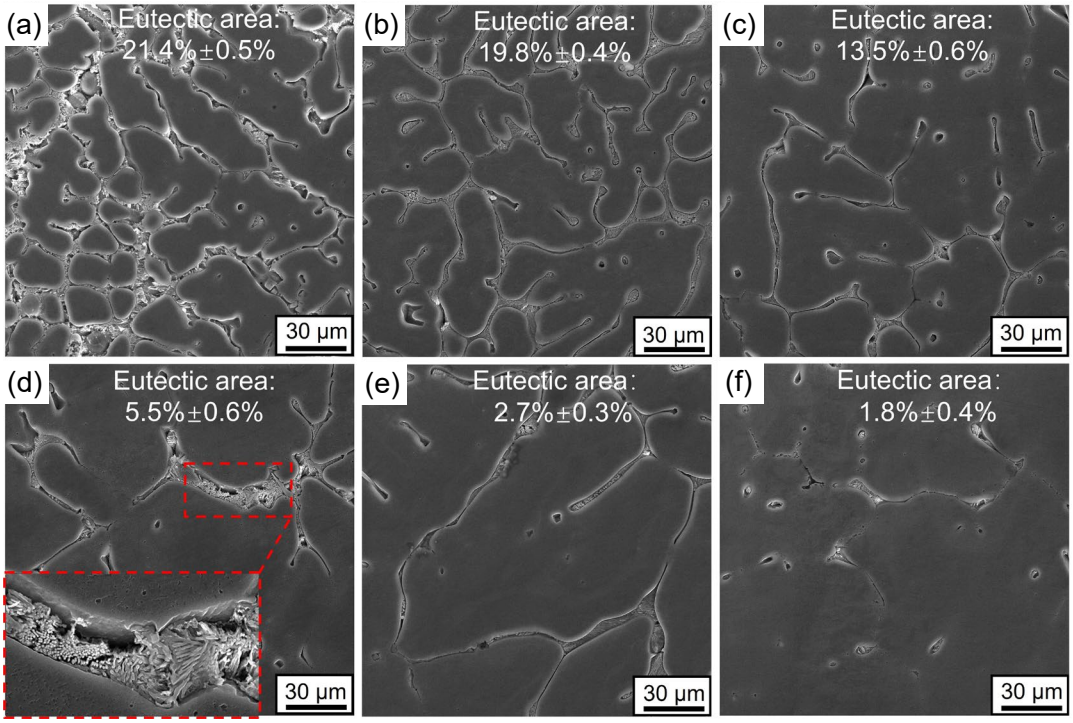

Fig. 4: SEM images of as-cast alloys: (a) Zn12; (b) Zn10; (c) Zn8; (d) Zn7; (e) Zn6; (f) Zn4

As illustrated in Fig. 5, the transverse macroscopic morphology [Figs. 5(a–f)] and longitudinal crack propagation depth [Figs. 5(a1–f1)] at the fracture surface of the cast alloy hot tearing test mold are presented. As demonstrated in Figs. 5(a–f), the flatness of the fracture surface varies considerably. With an increases in mass fractions of added solute elements (Zn, Mg, and Cu), the fracture surfaces become progressively flatter. As demonstrated in Figs. 5(a1–f1), the longitudinal crack propagation depth at the fracture surface exhibits a substantial increase with decreasing mass fractions of added solute elements (Zn, Mg, and Cu). For the Zn12 alloy, the longitudinal crack propagation depth is 2.21 mm. It increases to 4.95 mm for the Zn4 alloy. Such uneven fracture morphology and crack propagation depth reflect the shrinkage behavior of the alloy during fracture. At high solute contents, solute atoms restrict the shrinkage of the alloy, resulting in brittle fracture characteristics. The fracture surface is relatively flat with a shallow depth of longitudinal crack propagation, as shown in Figs. 5(a) and 5(a1). With decreasing solute content, the alloy exhibits a larger shrinkage strain. The improved ductility of the alloy leads to severe tearing at the fracture surface, which presents an uneven, gully-like morphology [(Fig. 5(f)] and a deeper crack propagation [Fig. 5(f1)]. A higher shrinkage rate of the alloy makes it more prone to cracking at locations with large cross-section variations in castings. Microscopically, shrinkage tends to occur preferentially at grain boundaries, resulting in intergranular cracking and the formation of hot tears.

Figure 6 shows the SEM images of the fracture surface at the mold breakage point during the hot tearing test, and the sampling location is indicated in Fig. 1. The eutectic T phases are clearly visible between the circular dendrites. The thickness of the intergranular liquid film (δ) at the hot tearing fracture surface was measured. In Zn12 alloy, the intergranular liquid film thickness is 3.85 μm. As the proportion of the eutectic microstructure within the α-Al matrix decreases, the thickness of the intergranular liquid film also diminishes. In Zn4 alloy, the intergranular liquid film thickness decreases to 1.97 μm. The thickness of the intergranular liquid film significantly influences the alloy's susceptibility to hot tearing at this stage: a thick liquid film accommodates greater strain, delays film rupture, and consequently enhances the alloy's resistance to hot tearing to a certain extent. Therefore, a thick intergranular liquid film reduces the alloy's susceptibility to hot tearing.

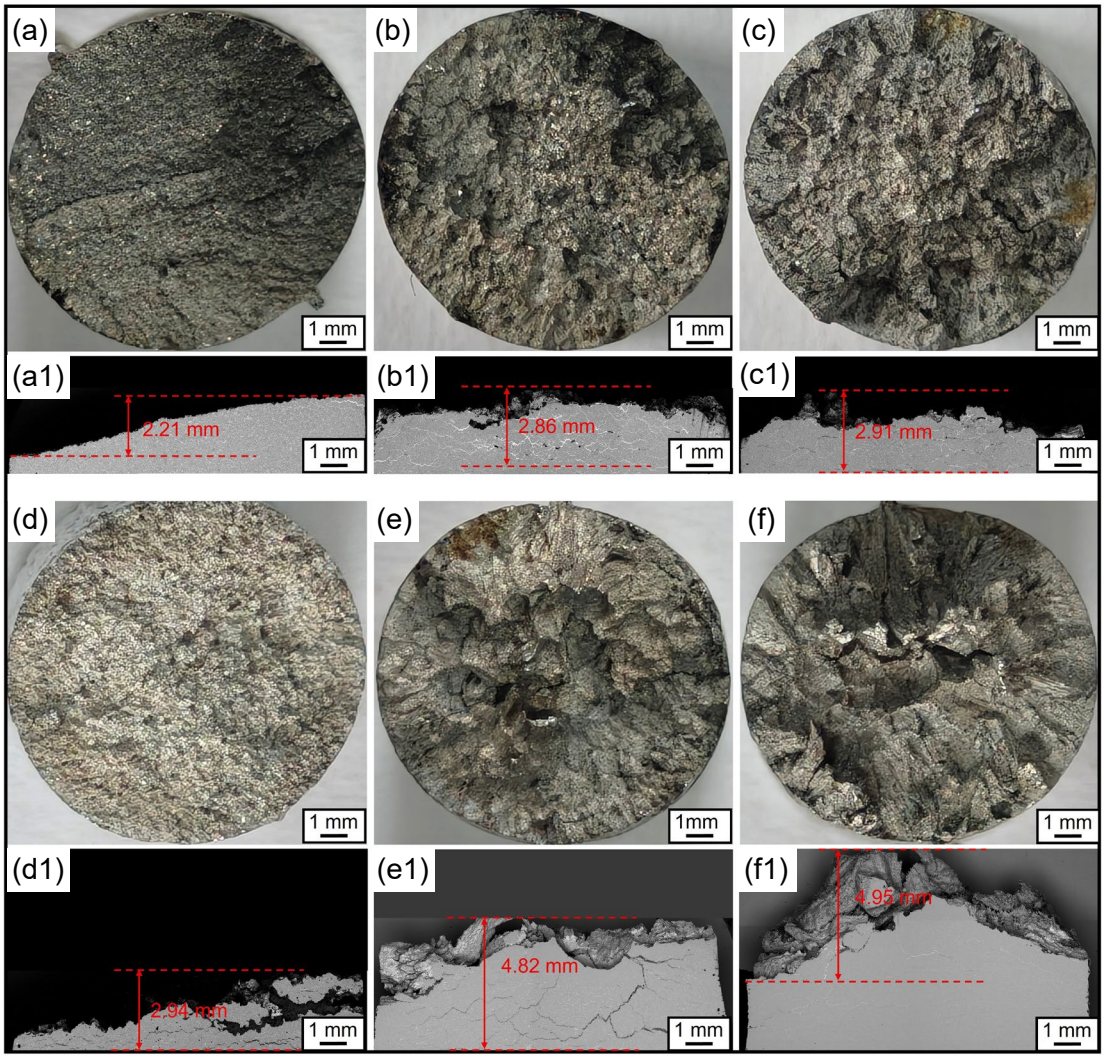

Fig. 5: Macroscopic morphology of transverse fracture surfaces (a–f) and longitudinal crack propagation depth (a1–f1): (a, a1) Zn12; (b, b1) Zn10; (c, c1) Zn8; (d, d1) Zn7; (e, e1) Zn6; (f, f1) Zn4

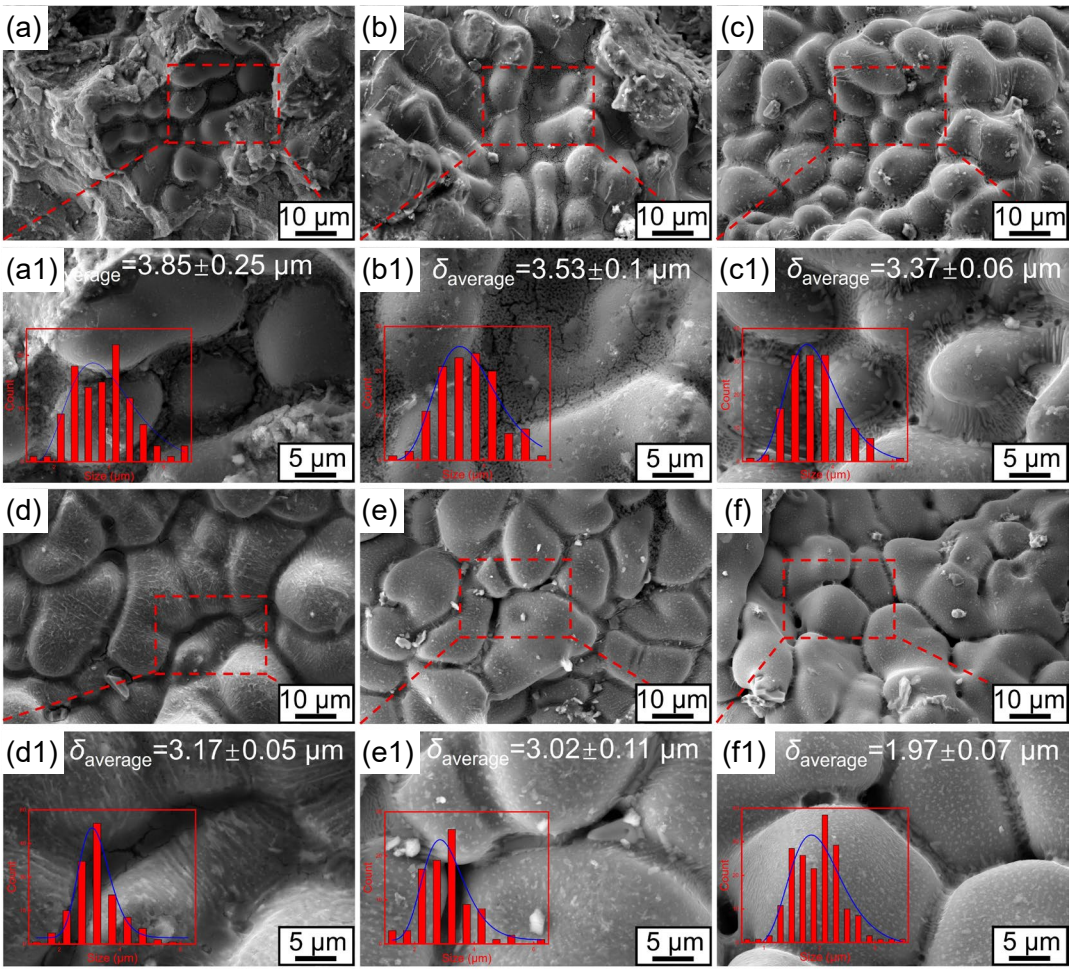

Fig. 6: Intergranular liquid film thickness at the fracture surface of alloys with different eutectic contents: (a, a1) Zn12; (b, b1) Zn10; (c, c1) Zn8; (d, d1) Zn7; (e, e1) Zn6; (f, f1) Zn4

3.2 Microstructure and mechanical properties after heat treatment

In all the experimental alloys, the type of eutectic phases remains unchanged, only their fraction varies. Since the phase types are identical, the characteristic reaction temperatures do not shift significantly. Therefore, only the Zn7 alloy, which has an intermediate eutectic content, was selected as a representative for determining the solution temperature. Figure 7 reveals two distinct endothermic peaks during the alloy's heating process. The lower-temperature peak corresponds to the low-melting-point eutectic microstructure, and the higher-temperature peak originates from the high-melting-point α-Al phase. According to DSC results, the alloy begins to partially melt at 478.6 °C. This represents a critical temperature point, known as the overburning onset temperature. Therefore, the solution treatment temperature is set at 475 °C. This temperature maintains a sufficient distance from the eutectic melting point while remaining within a sufficiently high temperature range.

Figure 8 shows the SEM results of the Zn7 alloy after different solution treatment times at 475 °C. As the solution treatment time increases from 10 h to 40 h, the area of the eutectics in the alloy decreases from 9.1% to 0.35%. Compared to the as-cast microstructure, the eutectic microstructural edges appear smoother after solution treatment, and the area of large eutectic domains decreases. This is because, during solid-state diffusion, solute atoms typically begin to dissolve into the α-Al matrix from the eutectic microstructural edges. Due to limited solubility in the α-Al matrix, solute atoms (Zn, Mg, and Cu) can only diffuse a finite distance in a short amount of time. Therefore, at a constant temperature, more time is required for solute atoms to fully dissolve into the α-Al matrix and form a supersaturated solid solution. However, when the solution treatment time increases from 30 h to 40 h, the dissolution rate of the eutectic phase into the matrix exhibits a significant

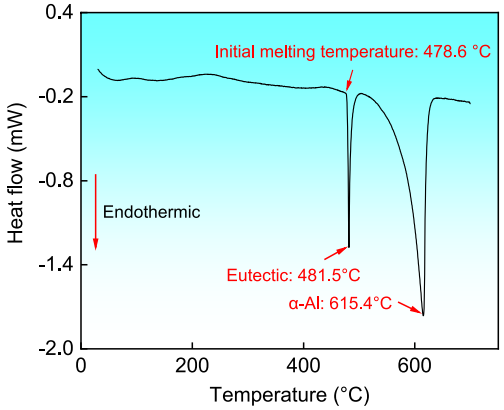

Fig. 7: DSC curve of Zn7 alloy

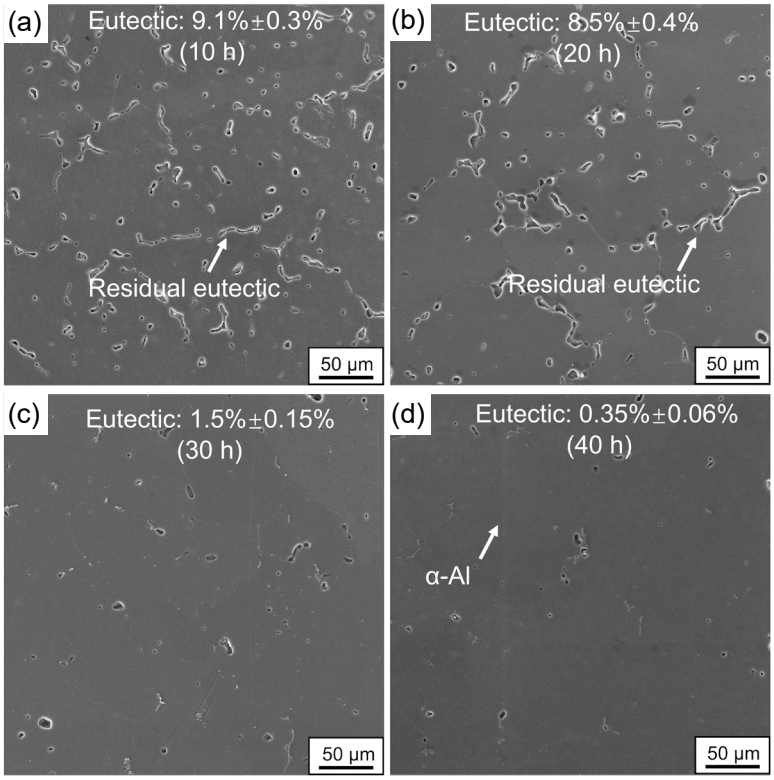

Fig. 8: SEM images of Zn7 alloy solution treated at 475 °C for different times: (a) 10 h; (b) 20 h; (c) 30 h; (d) 40 h

decline. At this point, most of the second phases in the alloy disappear, leaving only a partial, micron-sized second phase. Compared to the 30 h treatment, the eutectic microstructure in the matrix after 40 h treatment remains nearly identical. However, a longer solution treatment subjects the grains to prolonged thermal exposure. Driven by grain boundary energy, this induces grain growth and increases grain size, which ultimately degrades the alloy's strength. Taking all these factors into account, the eutectic microstructure in the matrix can be considered fully dissolved after 30 h of solution treatment.

The SEM results of alloys containing varying solute atoms (Zn, Mg, and Cu) following 30 h of solution treatment at 475 °C are illustrated in Fig. 9. It is evident that eutectic microstructures of Zn12 alloy remain undissolved within the α-Al matrix. When the Zn content is reduced to below 8wt.%, the morphology undergoes significant alterations following solution treatment and the area fraction of the eutectic microstructure decreases. As the content of solute atoms (Zn, Mg, and Cu) decreases, the fraction of residual eutectic microstructure in the solution treated alloys also diminishes. Specifically, at Zn contents below 8wt.%, the eutectic microstructure in the matrix is essentially fully dissolved into the α-Al matrix [Figs. 9(d–f)], although micrometer-sized second phases can still be identified. The EDS surface scanning in Figs. 9(d–e) reveals the presence of Cu-rich phases (Area 1 and Area 2). The EDS surface scan depicted in Fig. 9(f) reveals that the presence of partial Fe impurity elements leads to the formation of elongated Fe-enriched phases within the alloy (Area 3). This phenomenon can be attributed to the negligible solubility of Fe in the aluminum matrix at room temperature, with a reported solubility of only 0.04%[27]. Consequently, Fe tends to accumulate in the final liquid phase during the solidification process. As the solidification process continues, the concentration of Fe in the residual liquid phase between dendrites increases exponentially, reaching concentrations that are tens of times higher than the average composition of the liquid. This process gives rise to the formation of needle-like $Al_{13}Fe_4$ or elongated Fe-rich phases. This phase is an uncontrollable hard and brittle phase, which is mainly governed by alloy purity and the introduction of impurities during the casting process. Consequently, the sharp edges of Fe rich phases readily induce stress concentration during tensile deformation, leading to crack initiation and significantly degrading the service performance of the alloy. Overall, the Zn4 alloy exhibits the lowest fraction of residual phases after solution treatment.

Figure 10 shows the age-hardness response curves of alloys with different eutectic content after aging at 165 °C for different solution holding times. The aging temperature was selected based on the typical aging process parameters for this alloy system, with the aim of comparing the properties of different compositions under the same heat treatment conditions. The aging hardness curves show that the Zn12 alloy has the highest hardness after aging for 4 h. Zn10, Zn7, and Zn4 alloys reach peak hardness after aging for 6 h. Meanwhile, Zn8 and Zn6 alloys reach maximum hardness after aging for 2 h. This phenomenon likely stems from the combined regulation of the aging process by the content of the solute elements (Zn, Mg, and Cu), which influences the stability of the GP zone (higher Zn content reduces its dissolution temperature) and diffusion rates.

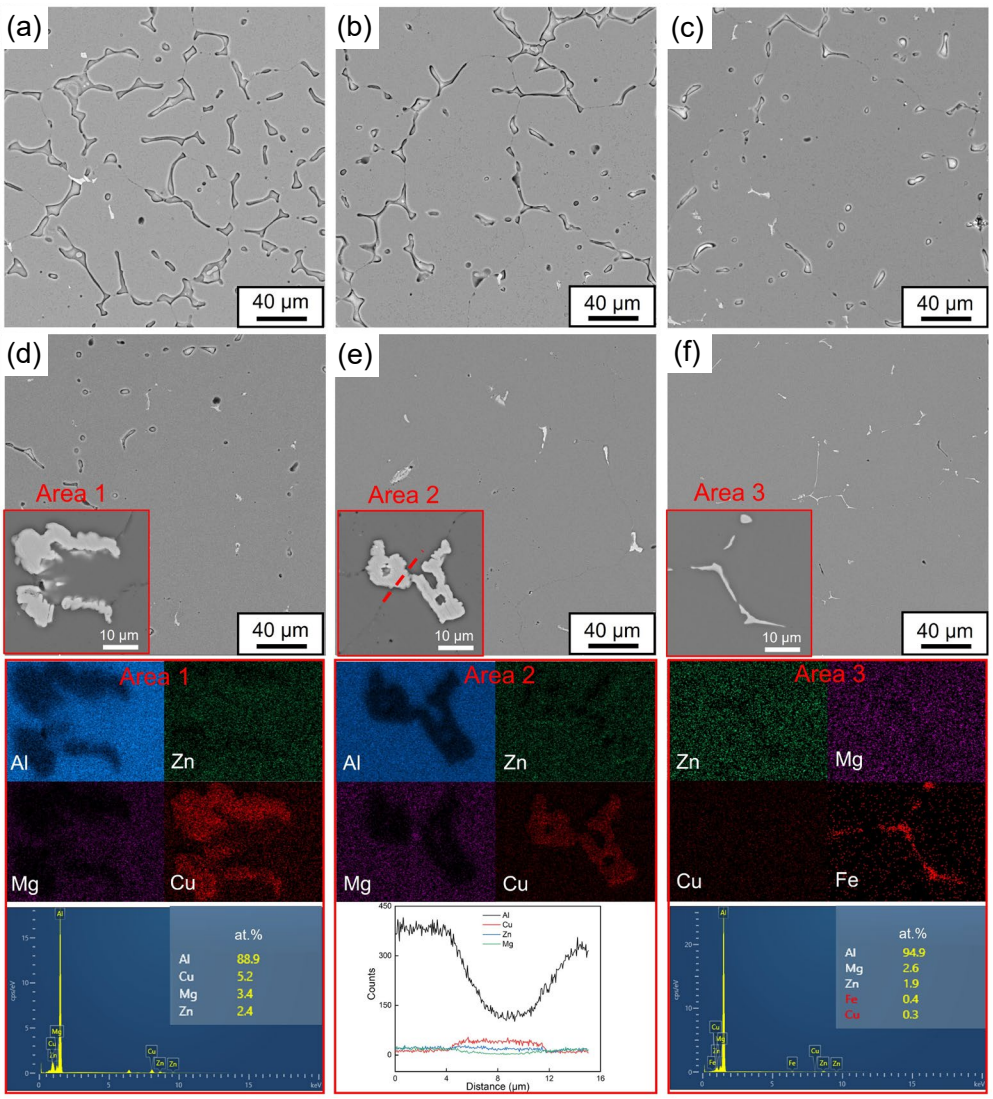

Fig. 9: Residual phases after solution treatment at 475 °C for 30 h: (a) Zn12; (b) Zn10; (c) Zn8; (d) Zn7; (e) Zn6; (f) Zn4

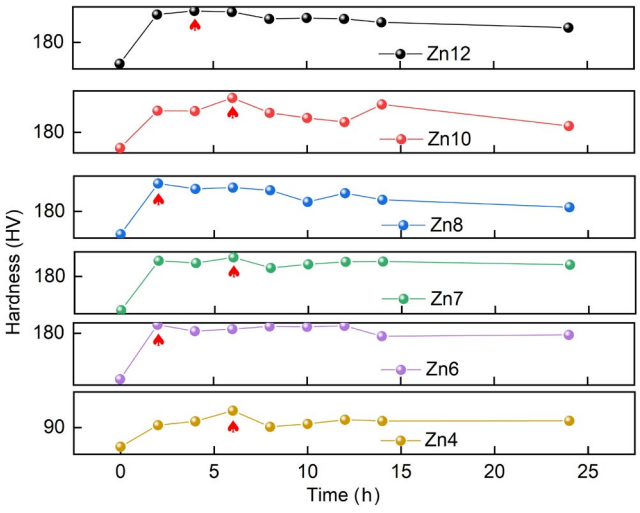

Fig. 10: Age-hardening curves of alloys with different eutectic content at 165 °C

Meanwhile, the hardness is also affected by the residual phases present in the matrix. For alloys with a low Zn/Mg ratio, the main precipitated phase is T phase[28]. The precipitation sequence in Al-Zn-Mg-Cu alloys is generally as follows: supersaturated solid solution→GP region (Zn/Mg enrichment)→T′ phase (metastable strengthening phase)→T phase (stable phase)[17]. However, in alloys with high Mg content, both the T phase and the η phase may precipitate simultaneously, thereby jointly enhancing the strength[29]. The introduction of Cu competes for solute sites, leading to the formation of S-Al_2CuMg or T-phases. During aging, the alloy undergoes three successive stages: underaging, peak aging, and overaging. The underaging stage is generally characterized by the formation of GP zones induced by solute atom clustering. In the peak aging stage, fine second-phase precipitates form, and the alloy achieves its maximum strength. The overaging stage corresponds to the coarsening of nanoscale second-phase precipitates, which results in the loss of coherency and consequently a reduction in the alloy's strength.

Figure 11 shows the XRD patterns of the samples after peak aging. Distinct diffraction peaks corresponding to the residual phases can be observed, which are identified as the T-$Mg_{32}(AlZn)_{49}$ phase and S-Al_2CuMg phase. From the magnified pattern in the range of 36°–40°, it is evident that the diffraction peak intensity of the residual T phase decreases with

decreasing eutectic content. The diffraction peak of the T phase completely disappears in the Zn6 alloy, confirming that the cast eutectic T phase can be fully dissolved into the α-Al matrix after 30 h of solution treatment at 475 °C. Meanwhile, a weak signal corresponding to the Al_2CuMg phase is also detected. As shown in Fig. 3, no diffraction peaks of the Al_2CuMg phases were detected in the XRD patterns. Owing to the relatively high cooling rate during casting, solute atoms such as Zn, Mg, and Cu readily reach the equilibrium eutectic point and form eutectic structures. In contrast, the aging process provides favorable thermodynamic and kinetic conditions for the decomposition of the supersaturated solid solution, enabling the slow diffusion, segregation, and nucleation of Cu and Mg solute atoms dissolved in the matrix, and eventually leading to the precipitation of the Al_2CuMg phase. Such nanoscale precipitates can effectively hinder dislocation motion and provide a certain strengthening contribution to the strength and hardness of the alloy, thereby exerting a positive regulatory effect on the overall mechanical properties of the aged alloy.

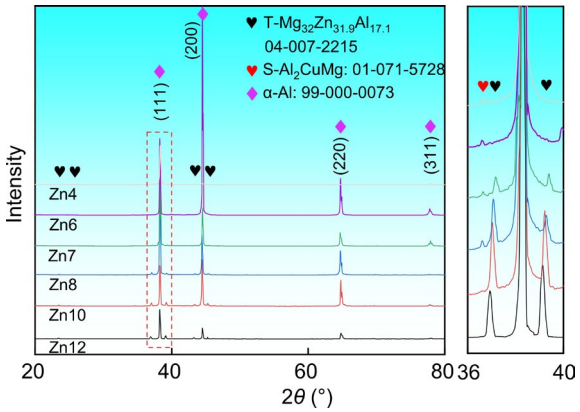

Fig 11: XRD results after aging treatment of alloys with different eutectic contents

The ultimate tensile strength and elongation of alloys with different eutectic contents in the peak-aged condition are shown in Figs. 12(a) and (b). The Zn6 alloy exhibits the best mechanical properties, with a tensile strength of 510 MPa and an elongation of 6.4%. Alloys with eutectic contents either higher or lower than that of the Zn6 alloy show inferior mechanical properties, but the underlying reasons differ. The Zn12, Zn10, Zn8, and Zn7 alloys contain a higher eutectic content, which cannot be fully dissolved during solution treatment, leading to more residual as-cast eutectic phases and consequently degrade their mechanical properties. It can also be clearly observed that the elongation of the these alloys is lower, which is attributed to the hindrance of dislocation motion by the residual eutectic phases. In contrast, the Zn4 alloy has a limited eutectic content; although the eutectic phase can be completely dissolved into the matrix during solution treatment, the amount of strengthening phases precipitated during subsequent aging is insufficient. As a result, the tensile strength of the Zn4 alloy is relatively low. However, a notable difference is that the reduced amount of residual phases in the Zn4 alloy leads to a significant increase in elongation.

Heat treatment tailors the mechanical properties of the alloy by modifying the size, distribution, and density of precipitates. The nanoscale precipitates formed during aging after solution treatment contribute predominantly to strengthening. These nanoscale precipitates effectively hinder dislocation motion, whereas larger secondary phases may become detrimental to mechanical properties. This is because larger secondary

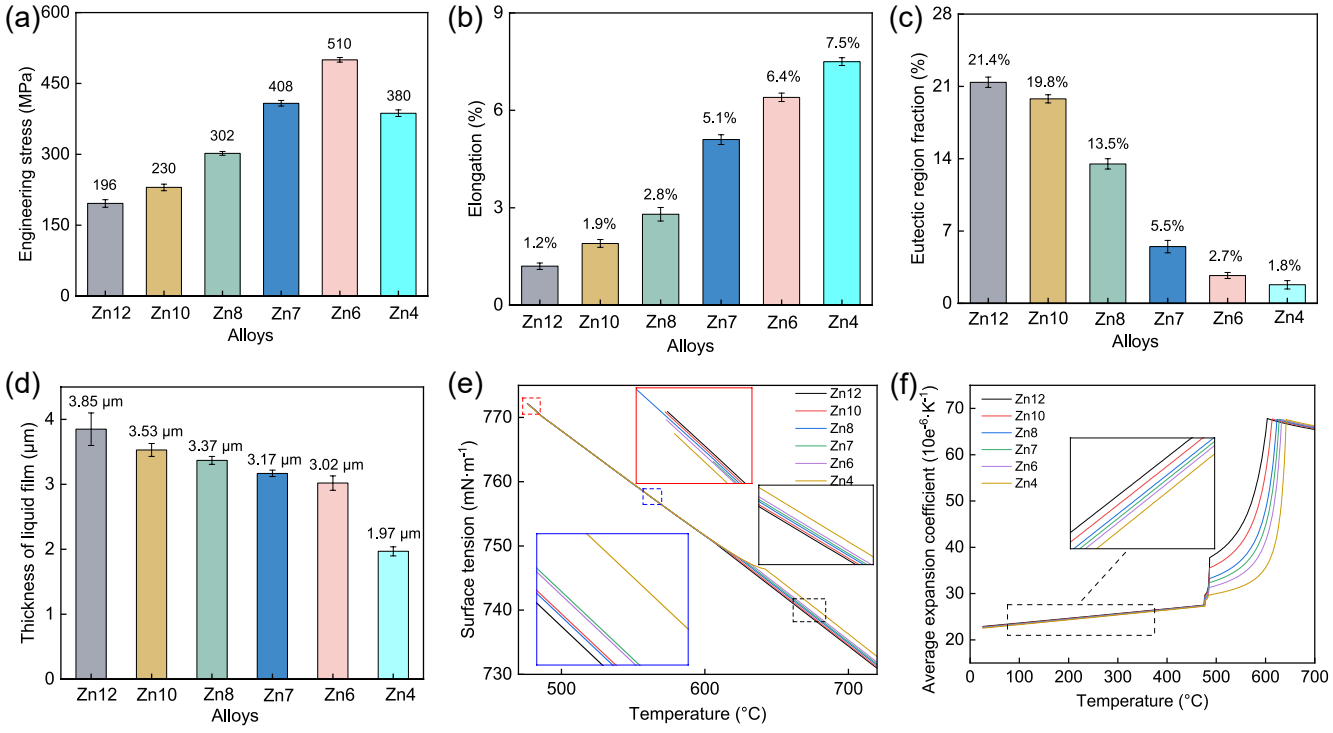

Fig. 12: Properties of alloys with different eutectic contents: (a) tensile strength; (b) elongation; (c) proportion of eutectics in as-cast state; (d) liquid film thickness at typical hot-tearing morphology; (e) surface tension; (f) average thermal expansion coefficient

phases exhibit poor deformation compatibility with the matrix during tensile loading, tending to cause stress concentration at interfaces and leading to cracking, thereby reducing the mechanical performance of the alloy. According to the residual phase analysis in Fig. 11, a higher as-cast eutectic content results in more residual phases after heat treatment, accompanied by poorer mechanical properties. This is mainly attributed to the limited solubility of Zn, Mg, and Cu in the α-Al matrix. SEM images of the alloys after solution treatment (Fig. 9) show that when excessive solute elements are added, the solute atoms cannot be fully dissolved into the α-Al matrix, sacrificing mechanical properties. Additionally, since Sc and Zr are added to all alloys, high-melting-point Al_3X (X=Sc, Zr) phases are formed in-situ during solidification, leading to grain refinement[30]. These Al_3X phases possess a coherent L12 structure, acting as effective Orowan barriers and Zener pinning sites, thereby contributing to grain refinement, suppression of elemental segregation, elimination of coarse secondary-phase particles, and inhibition of precipitate-free zones (PFZs) at grain boundaries[31].

Figures 12(c) and (d) present the statistical results of Figs. 4 and 6. The intergranular liquid film thickness is generally correlated with the hot-tearing susceptibility of the alloy: a thicker liquid film can accommodate larger strain, making the alloy less prone to hot tearing[26, 32-35]. Moreover, a higher eutectic content significantly contributes to the healing of hot tears during the final stage of solidification. The key casting performance (HTS) of the alloy is also related to surface tension and the coefficient of thermal expansion, as shown in Figs. 12(e) and (f). At elevated temperatures, alloys with higher eutectic contents exhibit lower surface tension. The lower surface tension reduces the wetting angle θ between the interdendritic liquid and the solid phase, thereby enhancing the fluidity and feeding capacity of the remaining melt. After complete solidification, a higher coefficient of thermal expansion makes the as-cast eutectic phases more prone to stress mismatch with the matrix, inducing microcracks. A higher eutectic content is beneficial to the casting performance of the alloy. However, limited by the maximum solid solubility of the α-Al matrix, a higher eutectic content is detrimental to mechanical properties. Therefore, the solid solubility limits of the eutectic-forming solute elements Zn, Mg, and Cu in the α-Al matrix represent a critical threshold, enabling both excellent casting performance and complete dissolution into the matrix to precipitate nanoscale phases for alloy strengthening.

Figure 13 illustrates the fracture morphology of the heat-treated alloys with different eutectic contents. A macroscopic analysis of the fracture morphology reveals that the fracture surfaces of all the six alloys are essentially perpendicular to the tensile stress direction. In alloys with higher eutectic contents [Figs. 13(a–c)], a substantial amount of lamellar structures is observed on the fracture surfaces, with no apparent dimples. Meanwhile, a small amount of residual eutectic structure can be seen in Figs. 13(a–c). The occurrence of intergranular fracture is mainly attributed to the presence of impurity elements at grain boundaries, which render the grain boundary strength lower than the matrix strength. Although the eutectic phases at grain boundaries can hinder grain deformation, the oversized intergranular phases induce dislocation pile up, leading to stress concentration and subsequent fracture. In alloys with lower eutectic contents [Figs. 13(d–f)], fine dimples and shear lips at the edges of the dimples are present on the fracture surfaces, exhibiting distinct characteristics of

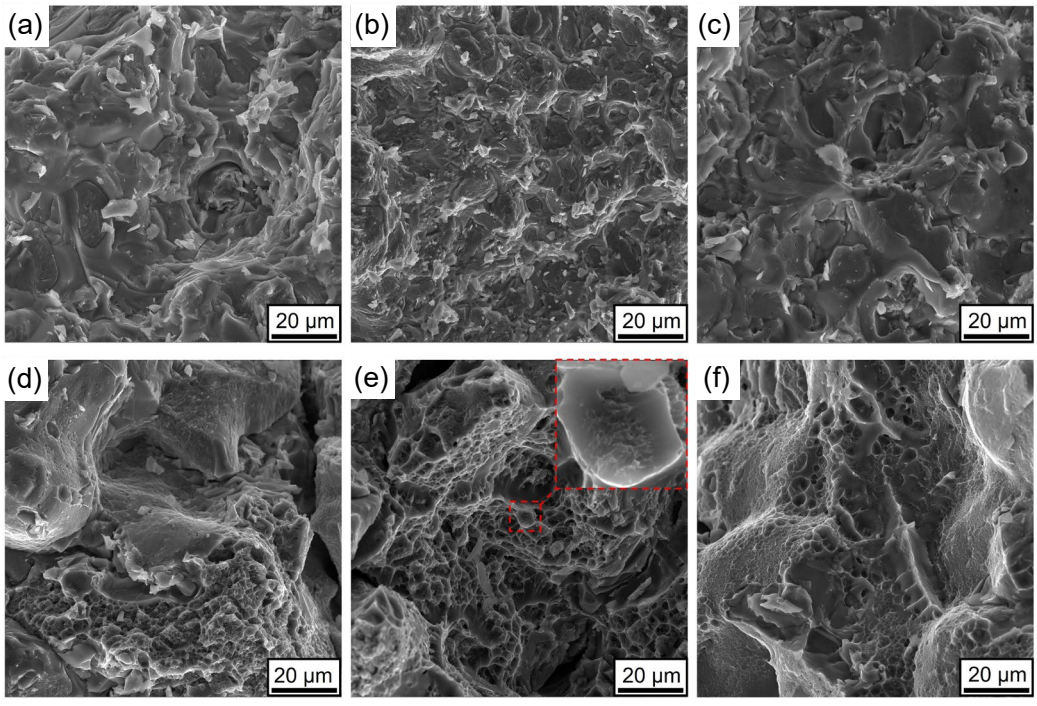

Fig. 13: Tensile fracture morphology of heat-treated alloys with different eutectic contents: (a) Zn12; (b) Zn10; (c) Zn8; (d) Zn7; (e) Zn6; (f) Zn4

plastic deformation fracture. In the Zn7, Zn6, and Zn4 alloys, the decrease in eutectic content results in a gradual increase in the number of dimples on the fracture surfaces, confirming that ductile fracture is the dominant failure mechanism. Owing to the lower eutectic content in the Zn4 alloy, the number of nanoscale precipitates formed after heat treatment is also lower. The reduced number of precipitates cannot fully impede dislocation motion; consequently, the Zn4 alloy exhibits better ductility but lower strength.

4 Conclusions

This study investigated the effects of eutectic phases content formed by adding different equi-proportions of solute elements (Zn, Mg, and Cu) on intergranular liquid film thickness, crack propagation depth, and mechanical properties of the alloy after heat treatment. The main conclusions are as follows:

(1) As the proportion of eutectic microstructure within the α-Al matrix decreases, the intergranular liquid film thickness also diminishes. The Zn12 alloy exhibits the largest intergranular liquid film thickness of 3.85 μm, while the Zn4 alloy shows the smallest thickness of 1.97 μm. A thick intergranular liquid film can accommodate greater strain, delaying film rupture and reducing the hot tearing susceptibility of the alloy.

(2) The longitudinal crack propagation depth at the alloy hot tearing fracture surface increases from 2.21 mm in the Zn12 alloy to 4.95 mm in the Zn4 alloy. The thickening of the intergranular liquid film allows it to withstand larger strain, making the film less prone to tearing, which consequently reduces the longitudinal crack propagation depth at the fracture surface.

(3) When solution treated at 475 °C, the residual eutectic phase fraction in the Zn7 alloy undergoes a decline from 9.1% at 10 h to 0.35% at 40 h. Under a constant alloy composition, the duration of solution treatment leads to a reduction in the proportion of residual eutectic phase within the α-Al matrix.

(4) Under identical solution treatment conditions, the peak age-hardened tensile strength rises from 196 MPa for the Zn12 alloy to 510 MPa for the Zn6 alloy, and then drops to 380 MPa for the Zn4 alloy. The elongation of the alloy increases from 1.2% for the Zn12 alloy to 7.5% for the Zn4 alloy.

(5) High contents of solute elements (Zn, Mg, and Cu) lead to the formation of a large number of eutectic phases, exceeding the solubility limit of the α-Al matrix and leaving a substantial amount of undissolved residual phases, which deteriorates the alloy's properties. In the alloy with the lowest eutectic content (Zn4 alloy), the amount of solute atoms dissolved into the α-Al matrix is limited, thereby reducing the number of strengthening precipitates and consequently enhancing the ductility of the alloy.

Acknowledgments

This work was financially supported by the National Natural Science Foundation of China (Grant number 52575391), the Science and Technology Major Project of Yunnan Province (Grant number 202502AB080012), and the project funds of "Xingdian Talent Support Program".

Conflict of interest

The authors declare that they have no known competing financial interests or personal relationships that could have appeared to influence the work reported in this paper.

References

[1] Zhang H, Rong L, Ma C, et al. Er and Zr microalloying and hot tearing susceptibility of Al-30Zn-2Cu high-zinc aluminum alloys. International Journal of Metalcasting, 2025, 20: 1081–1097.
[2] Yang M, Wang S, Zhang M, et al. Aging hardening and precipitation behavior of high Zn/Mg ratio Al-Zn-Mg alloys with and without Cu. Journal of Alloys and Compounds, 2025, 1022: 180017.
[3] Guo Y, Qi F, Wang Y, et al. An extended criterion for hot cracking susceptibility of Al-Li alloys. Engineering Failure Analysis, 2025, 171: 109348.
[4] Guo X, Liu Y, Zhao H, et al. Optimizing hot tearing susceptibility of Mg-1Ca alloy by pulsed magnetic fields: Experimental investigation and numerical simulation. Engineering Failure Analysis, 2025, 174: 109518.
[5] Xu H Y, Jia H F, Ji Z S, et al. Effect of La content on microstructure, tensile properties, and electrical conductivity of cast Al-Mg-Si-xLa alloys. China Foundry, 2025, 22(3): 385–394.
[6] Zhao H, Gault B, Ponge D, et al. Reversion and re-aging of a peak aged Al-Zn-Mg-Cu alloy. Scripta Materialia, 2020, 188: 269–273.
[7] Lin Y C, Zhang J L, and Chen M S. Evolution of precipitates during two-stage stress-aging of an Al-Zn-Mg-Cu alloy. Journal of Alloys and Compounds, 2016, 684: 177–187.
[8] Jo Y H, Jung H, Jeon S, et al. The effect of Zn content on tensile properties and fracture toughness of Al-Zn-Mg-Cu alloy. Journal of Materials Research and Technology, 2025, 36: 5696–5706.
[9] Wang Y, Chen S, Zhang Y, et al. Microstructure evolution and enhancement mechanism of a novel laser cladded Al-Mg-Zn-(Cu-Co-Er-Zr) alloy based on material genetic design. Materials Characterization, 2025, 223: 114984.
[10] Yang M, Lu F, Zhou S, et al. Effect of Cu on precipitation hardening and clustering behavior of Al-Zn-Mg alloys in the early stage of aging. Materials Characterization, 2025, 219: 114632.
[11] Sun Z, Hao S, Duan H, et al. Microstructure, strength and corrosion resistance in an Al-Zn-Mg-Cu alloy after artificial aging and subsequent long-term natural aging. Journal of Alloys and Compounds, 2025, 1036: 181915.
[12] Fan W X, Bai Y, Hao H, et al. Al-CeO_2-Mg refiner on grain refinement, cast fluidity and mechanical properties of AZ91 alloy. China Foundry, 2024, 21(6): 667–675.
[13] Peng J, Yuan S, Wang W, et al. Achieving high strength and plasticity in a novel Al-Zn-Mg-Cu-Y-Cr alloy via thermomechanical treatment. Materials Science and Engineering: A, 2025, 941: 148623.
[14] Dai Y, Yan L, Sun S, et al. In-depth investigation of microstructural evolution induced by Sc, V, and Ni microalloying in Al-Zn-Mg-Cu alloy during hot compression. Materials & Design, 2025, 253: 113857.

[15] Akuata C K, Belkacemi L T, and Zander D. Revisiting Ag addition in 7xxx aluminum alloys: Insights into its impact on the microstructure and properties of an Al-Zn-Mg-Cu-Zr alloy with a Zn/Mg ratio of 4. Materials Characterization, 2024, 215: 114186.
[16] Han Q, Zhao S, Tang Y T, et al. FCC/B2 phase boundary variant-sensitive fatigue cracking in a eutectic high entropy alloy at high temperature. International Journal of Plasticity, 2025, 185: 104223.
[17] Tan P, Qin J, Quan X, et al. Co-strengthening of the multi-phase precipitation in high-strength and toughness cast Al-Cu-Zn-Mg alloy via changing Zn/Mg ratios. Materials Science and Engineering: A, 2023, 873: 145024.
[18] Li H, Zhu C, Gu X, et al. Understanding the strength increment of Al-Zn-Mg-Cu aluminum alloys by enhanced solution-treatment (EST). Materials Science and Engineering: A, 2024, 903: 146677.
[19] Yang Y M, Tang X C, Li Y F, et al. Effect of heat treatment on microstructure and mechanical properties of a novel Al-Zn-Mg-Cu alloy. China Foundry, 2025, 22(3): 292–300.
[20] Tang S, Wu X, Cao L, et al. Anomalous precipitation behavior in T-phase strengthened Al-Mg-Zn(-Cu) alloys: Effects of aging temperatures and Cu contents. Materials Science and Engineering: A, 2025, 933: 148287.
[21] Huang R, Yang H, Zheng S, et al. The evolution mechanism of the second phase during homogenization of Al-Zn-Mg-Cu aluminum alloy. Materials & Design, 2023, 235: 112395.
[22] Villanueva E, Vicario I, Crespo I, et al. Development of a new ductile heat-treated multi-component aluminium by HPDC with high-performance properties for temperature applications. Journal of Alloys and Compounds, 2025, 1020: 179146.
[23] Li K, Wang Y, Su R, et al. Cyclic non-isothermal aging: An aging method to simultaneously improve mechanical properties and corrosion resistance of Al-Zn-Mg-Cu alloys. Journal of Alloys and Compounds, 2025, 1022: 179970.
[24] Lin Y, Wang L, Geng B, et al. Effect of Ni addition on the hot tearing susceptibility of Al-Zn-Mg-Cu alloys. Metallurgical and Materials Transactions: A, 2025, 56: 3771–3787.
[25] Lin Y and Wang L. Effect of Mg content on the hot tearing susceptibility of Al-Zn-Mg-Cu alloys. International Journal of Metalcasting, 2025, 19: 3681–3693.
[26] Li P, Sui Y, Shen W, et al. High content of solute elements (Zn, Mg, Cu) increases the hot tearing susceptibility resistance of Al-Zn-Mg-Cu alloys. Journal of Alloys and Compounds, 2025, 1022: 179852.
[27] Mohammed W, Chen X, Ponge D, et al. Thermodynamics-guided design of sustainable secondary Al-Si alloys for enhanced Fe-impurity tolerance and optimized Mn doping. Acta Materialia, 2025, 289: 120932.
[28] Yang X B, Chen J H, Liu J Z, et al. A high-strength AlZnMg alloy hardened by the T-phase precipitates. Journal of Alloys and Compounds, 2014, 610: 69–73.
[29] Zou Y, Wu X, Tang S, et al. Co-precipitation of T′ and η′ phase in Al-Zn-Mg-Cu alloys. Materials Characterization, 2020, 169: 110610.
[30] Wang C, Gao W, Min J, et al. Stabilization of metastable η' phase in Al-Zn-Mg-Cu-Ti alloy fabricated by laser direction energy deposition. Materials Characterization, 2025, 228: 115368.
[31] Li Q, Qiao J, Zhao A, et al. Reversing the strength-ductility trade-off in Al-Zn-Mg-Cu alloys via trace Sc microalloying and $L1_2$ dispersoid precipitation. Materials Science and Engineering: A, 2025, 945: 149054.
[32] Wang S, Yue C, Kang J, et al. Effect of rare earth Y on liquid film of later solidification stage and hot tearing of spherical Al-Cu-Mg alloy. Journal of Materials Engineering and Performance, 2024, 34: 6035–6045.
[33] Zhou R, Fang X, Yu J, et al. Effect of intergranular liquid film characteristics on hot tearing formation of hypereutectic Al-Si alloy. International Journal of Metalcasting, 2024, 19: 2584–2592.
[34] Zhou R, Fang X, Zhang K, et al. Relationship between characteristics of liquid film and hot tearing phenomena during solidification of hypereutectic Al-Si alloy. Journal of Materials Science, 2025, 60: 6987–7001.
[35] Zhou Z, Fang X, Ma Z, et al. Study on stress-strain and hot tearing of liquid film between single grains of high-silicon aluminum alloy. International Journal of Metalcasting, 2024, 19: 1378–1387.